Optical ranging and localization at beyond the coherence length of lasers

M. Mert Bayer, Berken Utku Demirel, Ataberk Atalar, Xun Li, Haoyu Xie, et al.

M. Mert Bayer, Berken Utku Demirel, Ataberk Atalar, Xun Li, Haoyu Xie, Ozdal Boyraz, "Optical ranging and localization at beyond the coherence length of lasers," Proc. SPIE 12438, AI and Optical Data Sciences IV, 124380H (15 March 2023); doi: 10.1117/12.2647159

SPIE.

Event: SPIE OPTO, 2023, San Francisco, California, United States

Optical Ranging and Localization at Beyond the Coherence Length of Lasers

M. Mert Bayer[a], Berken Utku Demirel[a], Ataberk Atalar [a], Xun Li [a], Haoyu Xie [a], Ozdal Boyraz*[a]
[a]Electrical Engineering and Computer Science Department, University of California, Irvine, CA 92697 USA

ABSTRACT

Long-distance ranging in existing coherent lidar techniques suffer from the coherence length of lasers. Here we present a coherent multi-tone continuous-wave (MTCW) lidar technique that performs single-shot simultaneous ranging and velocimetry with a high resolution at distances far beyond the coherence length of a CW laser, without frequency/phase sweeping. The proposed technique utilizes relative phase accumulations at phase-locked RF sidebands and Doppler shifts to identify the range and velocity of the target after a heterodyne detection of the beating of the echo signal with an unmodulated CW optical local oscillator (LO). The predefined RF sidebands enable ultra-narrow-bandwidth RF filters in the analog or digital domain to suppress noise and achieve high SNR ranging and velocimetry. Up-to-date, we demonstrated that the MTCW-lidar could perform ranging ×500 beyond the coherence length of the laser with <1cm precision. In a quasi-CW configuration, >1km ranging is realized with <3cm precision. Moreover, we incorporate machine-learning algorithms into MTCW-lidar to identify the reflections from multiple targets and improve the range resolution. Since relative phases of RF-sidebands are utilized for ranging, and common phase noises can be suppressed in signal processing, we show that the LO in heterodyne detection does not have to be the same laser source. Hence a separate free-running laser can be used. This approach paves the way for novel optical localization. To prove the concept, we present that a receiver with a free-running CW LO can determine its relative distance to a remote transmitter at 1.5km away with a <5cm accuracy.

Keywords: Lidar, machine learning, optical reflection measurement

1. INTRODUCTION

Over the years, sensor fusion generated a tremendous amount of data that ordinary computational methods cannot handle[1]. Machine learning (ML) and artificial intelligence (AI) emerged as natural gateways to reduce data clogs and effectively utilize details that are overlooked in traditional methods[2,3]. While ML algorithms can now identify, sort, and route data without going through extensive observations, AI algorithms make decisions on the nature of data and act on them without human intervention[4]. Despite vast developments in AI and ML in other areas, optical lidar-based sensing technologies seldom utilize AI and ML algorithms for forestry and autonomous vehicle applications[5–10].

In particular, light detection and ranging (lidar) are investigated and implemented in real-life applications such as vehicle crash prevention, autonomous driving, forestry and oceanography, and precision measurements[11–14]. Various lidar techniques are developed, including direct light detection of laser pulse propagation that facilitates time-of-flight measurements[15–18], as well as coherent detection via amplitude-modulated, phase-modulated, or frequency-modulated continuous-wave (CW) light[19–22]. The coherent lidars provide a detection scheme limited by the shot noise, hence improving the signal-to-noise ratio (SNR) of the detection and enhancing the precision of the measurements[23]. On the other hand, CW lidars rely on phase or frequency sweep of the light, which limits the potential single-shot operations for fast-moving platforms such as CubeSats or airborne lidars[24]. Even though the CW configuration enhances the range resolution and provides simultaneous velocimetry capability via the Doppler effect[25], the CW lidars are hindered by the laser phase noise, which dictates the maximum detection range, in other words, the coherence length of the laser[26].

To remedy the aforementioned limitations to coherent lidars, we previously developed and demonstrated the phase-based multi-tone continuous-wave (PB-MTCW) lidar, which can perform ranges far beyond the coherence length limitations[27]. In this technique, we split the output of a CW laser and amplitude modulate one arm with multiple phase-locked radio-frequencies (RF), while the unmodulated branch is kept as a local oscillator (LO) for shot noise-limited heterodyne detection. In the echo signal, each RF tone accumulates a different phase with respect to the tone frequency and the target distance. Since the tones are embedded into the same optical carrier, it is possible to cancel out the common phase-noise components by RF mixing the individual detected tones with each other. Hence, the phase-noise-free terms

AI and Optical Data Sciences IV, edited by Bahram Jalali, Ken-ichi Kitayama,
Proc. of SPIE Vol. 12438, 124380H · © 2023 SPIE
0277-786X · doi: 10.1117/12.2647159

can be utilized via position triangulation algorithms by utilizing the plurality of the tone frequencies and tone phases[28,29]. Furthermore, similar to the other coherent lidars, the PB-MTCW technique can utilize the Doppler frequency shifts to compute the target velocity simultaneously with the ranging, as well. We have demonstrated that the PB-MTCW technique can perform ranging ×500 more than the coherence length of CW lasers with <1cm precision. The same technique is also used for clock-free localization of targets for autonomous vehicles.

All of the developments in the lidar field mainly focus on one of the three measurable quantities: Amplitude, frequency, or phase[20,30]. Here, we hypothesize that by training an ML algorithm using all the aspects of the stable RF tones, which includes the phase, frequency, and amplitude information, it is possible to improve the measurement accuracy and provide a solution to multi-path interference and multi-surface reflections[22,31]. This hypothesis is true when a complex target geometry is placed in front of the beam. In this work, we show the enhancement of the PB-MTCW technique using ML algorithms and pattern recognition techniques. In particular, we develop ML algorithms that utilize all three measurable parameters to identify complex target structures. When the lidar aperture concurrently receives two multi-tone modulated echo signals from multiple surfaces in the same line of sight, the RF tones will realize amplitude variations due to light interference. These amplitude variations differ based on the target distances and tone frequencies. By utilizing the relative amplitude variations between the individual tones, it is possible to estimate the existence of multiple targets, as well as the distances of both targets, using the pre-trained ML algorithm. We demonstrate the capability of the technique with simulation and experimental results. We show that we can estimate the multi-path interference with 94% accuracy, and we can find the position of multiple targets with <5cm error. Similarly, the ML algorithm can verify the single reflection with >97% accuracy. Moreover, we illustrate that the ML algorithm yields an average mean square error of ~1.1mm, hence enhancing the ranging accuracy of the PB-MTCW lidar. This approach has the potential to resolve one of the main challenges of existing lidar techniques, which is multi-path interference and to facilitate precise navigation and localization applications[32].

2. PHASE-BASED MULTI-TONE CONTINUOUS-WAVE LIDAR

2.1 Concept

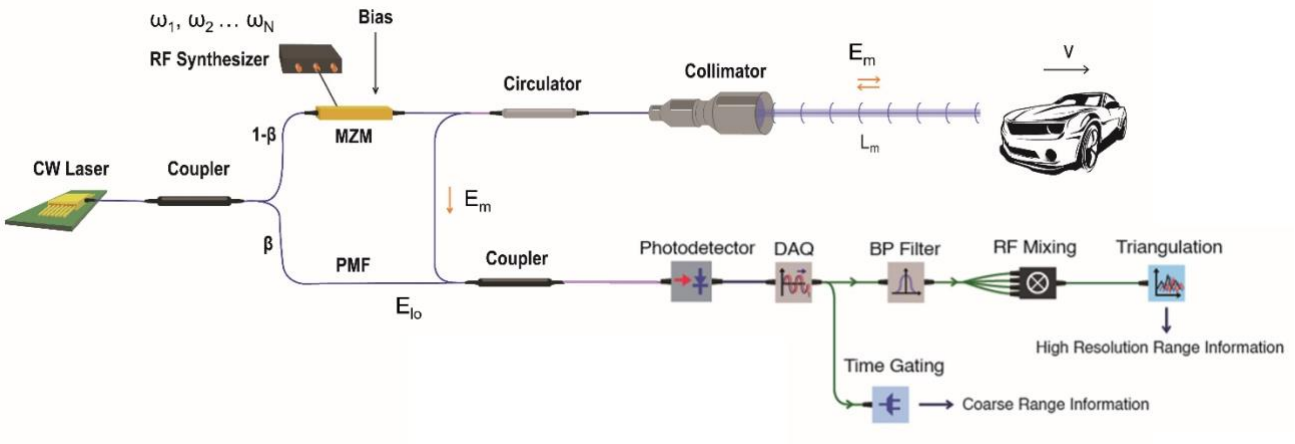

Figure 1. Working principle of the Phase-Based Multi-Tone Continuous Wave lidar.

The previously demonstrated Phase-Based Multi-Tone Continuous Wave lidar (PB-MTCW) technique involves modulating a continuous wave laser with multiple phase-locked radio-frequency tones each having a frequency of f_i using a Mach-Zehnder modulator[27]. The accumulated phases of these tones are encoded in the echo signal after light propagation. Each modulation tone will accumulate a phase based on the target distance, L_m, and speed of light, c, as $\phi_i^{range} = \left(2L_m\omega_i\right)/c$, where $\omega_i = 2\pi f_i$. The received signal is then further interfered with by an unmodulated local oscillator (LO) to acquire the beat notes and realize a shot-noise limited detection. By utilizing the apriori knowledge of the selected tone frequencies, each tone is filtered with low bandwidth bandpass filters. The individual tones are further RF mixed with one another to yield the phase-noise-free intermediate frequencies (IF). Since there are multiple IF terms with particular phases, it is possible to triangulate the target position using the phase and frequency information of the resultant IFs as illustrated in Figure 1.

2.2 Theoretical Model

Theoretically, the electric field (E-field) of the CW laser is formulated as $E_{laser} = A_0 \exp(j\omega_0 t + j\phi_0)$, where $A_0 = \sqrt{P_{out}}$ is the amplitude, ω_0 is the optical carrier frequency and ϕ_0 is the initial phase of the source laser. The laser is then split into two by a coupler with a β/(1-β) power splitting ratio. The unmodulated local oscillator is formulated as in Eq.(1) by also considering fiber attenuation (α_f) and laser phase noise ($\phi_n(t-\tau_{LO})$), where τ_{LO} is the propagation time in the local oscillator branch.

$$E_{LO} = A_0 \alpha_f \sqrt{\beta} \exp(j\omega_0 t + j\phi_0 + j\phi_n(t-\tau_{LO})) \tag{1}$$

The E-field of the echo signal is presented in Eq.(2) after defining the linear attenuation coefficient (α_m) related to the potential scattering, collection, and/or back coupling losses.

$$\begin{aligned} E_m = {} & \frac{A_0}{2\sqrt{2}} \alpha_m \alpha_f \sqrt{1-\beta} \exp\left[j\omega_0 t + j\phi_0 + j\omega_0 \frac{2L_m}{c} + j\phi_n(t-\tau) \right] \\ & - \frac{mA_0}{4\sqrt{2}} \alpha_m \alpha_f \sqrt{1-\beta} \sum_{i=1}^{N} \left(\begin{array}{l} \exp\left[j(\omega_0+\omega_i)t + j\phi_0 + j\phi_i^{RF} + j(\omega_0+\omega_i)\frac{2L_m}{c} + j\phi_n(t-\tau) \right] \\ + \exp\left[j(\omega_0-\omega_i)t + j\phi_0 - j\phi_i^{RF} + j(\omega_0-\omega_i)\frac{2L_m}{c} - j\phi_n(t-\tau) \right] \end{array} \right) \end{aligned} \tag{2}$$

Here, $\tau = 2L_m / c$ is the time of propagation and $\phi_n(t-\tau)$ is the laser phase noise related with τ that is when the laser beam first exists the MZM. Since the defined phase noise term is related to the carrier, the same noise term will be carried by every modulation frequency. The E_m and E_{LO} are combined via a Y-coupler and the photocurrent is achieved as $I_{pd} = R(E_m + E_{LO}) \cdot (E_m + E_{LO})^*$. The final I_{pd} after the interference of the local oscillator with the echo signal from a stationary target is shown in Eq.(3), where the laser phase noise difference of E_m and E_{LO} is represented as $\Phi(t,\tau,\tau_{LO}) = \phi_n(t-\tau_{LO}) - \phi_n(t-\tau)$ [33].

$$\begin{aligned} I_{pd} = {} & RA_0^2\alpha_f^2\beta + \frac{3RA_0^2\alpha_m^2\alpha_f^2(1-\beta)}{16} + \frac{RA_0^2\alpha_m\alpha_f^2\sqrt{\beta}\sqrt{1-\beta}}{\sqrt{2}} \cos\left(\omega_0 \frac{2L_m}{c} + \Phi(t,\tau,\tau_{LO}) \right) \\ & - \frac{RmA_0^2\alpha_m\alpha_f^2\sqrt{\beta}\sqrt{1-\beta}}{2\sqrt{2}} \left[\begin{array}{l} \sum_{i=1}^{N} \cos\left(\omega_i t + (\omega_0+\omega_i)\frac{2L_m}{c} + \phi_i^{RF} + \Phi(t,\tau,\tau_{LO}) \right) \\ + \sum_{i=1}^{N} \cos\left(\omega_i t - (\omega_0-\omega_i)\frac{2L_m}{c} - \phi_i^{RF} - \Phi(t,\tau,\tau_{LO}) \right) \end{array} \right] \\ & + \frac{RmA_0^2\alpha_m^2\alpha_f^2(1-\beta)}{8} \left[\sum_{i=1}^{N} \cos\left(\omega_i t + \omega_i \frac{2L_m}{c} + \phi_i^{RF} \right) + \sum_{i=1}^{N} \cos\left(\omega_i t + \omega_i \frac{2L_m}{c} - \phi_i^{RF} \right) \right] \\ & + \frac{Rm^2A_0^2\alpha_m^2\alpha_f^2(1-\beta)}{8} \sum_{i=1}^{N} \cos\left(2\omega_i t + \omega_i \frac{4L_m}{c} \right) \end{aligned} \tag{3}$$

Using the resultant photocurrent, it is possible to extract the individual tones by applying narrow bandwidth bandpass filters centered at each frequency. Then, we can RF mix the filtered tones to annihilate the common phase-noise terms caused by the optical carrier. After the RF mixing, two of these individual tones at ω_i and ω_j ($i \neq j$) yields the IF expressed as $A_i A_j \cos(\Delta\omega_{i,j} t \pm \Delta\phi_{i,j})$, where $\Delta\phi_{i,j}$, and $\Delta\omega_{i,j}$ are the phase and frequency differences of i^{th} and j^{th} tones, respectively. The range of the target can further be defined as $L_m = (2\pi n + \Delta\phi_{i,j})c / \Delta\omega_{i,j}$, where n is an integer. The cyclic nature of the phase's modulo-2π behavior will result in periodic range estimation. To achieve accurate range information, it is necessary to have redundancy through the use of multiple agents, which is provided by the plurality of modulation tones. The solution of L_m for each $\Delta\omega_{i,j}$ should converge to a single value for a particular n. To find the common solution, we developed a triangulation algorithm that generates all the potential solutions for each IF by sweeping the integer values of n. Then we estimate the target range by acquiring the common solution for all IFs[27,28].

2.3 Experimental Setup

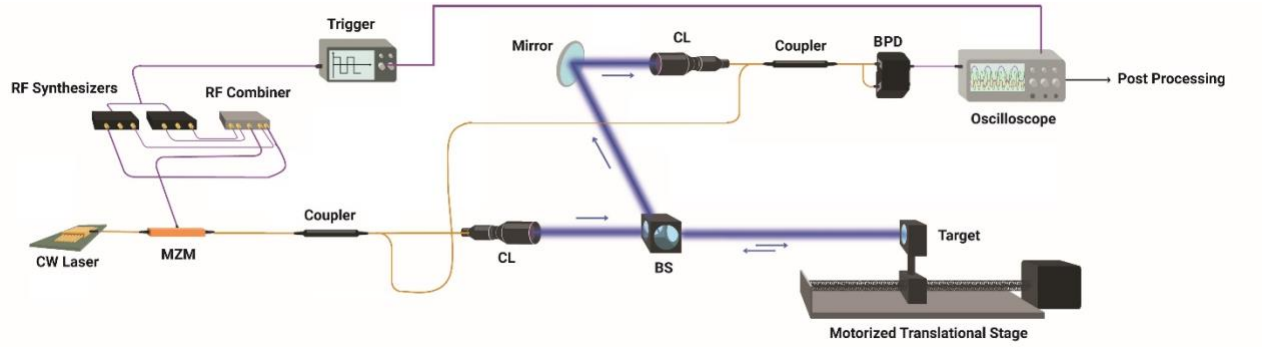

Figure 2. The PB-MTCW experimental setup. Mach-Zehnder Modulator (MZM), collimator (CL), beamsplitter (BS), and balanced photodetector (BPD).

The experimental setup shown in Figure 2 is used to measure the range of a static target. A CW laser with a <100kHz linewidth at 1064nm (RPMC Lasers - R1064SB0300PA) is modulated using an MZM (iXblue – NIR-MX-LN series), which is optimized for 1064nm and has a 30dB extinction ratio, with four frequencies at 300, 500, 890, and 1350MHz. These frequencies are carefully selected to prevent overlap or second harmonic mixing. The tones are generated by phase-locked RF synthesizers (Windfreak Technologies - SynthHD (v2)) and triggered by a 10MHz common clock that also triggers the oscilloscope. The target reflector is placed on a motorized translational stage, and the target is moved in 2cm steps on the stage during multiple trials. The modulated light is transmitted to the free space using a (CL) and coupled back to another collimator for collection. The collected signal interferes with the LO through an optical Y-coupler. The final light signal is split into two and fed to a high-speed balanced photodetector (BPD) (PDB482C-AC), which has a bandwidth of 2.5GHz and a noise equivalent power of 12pW/Hz$^{1/2}$. The initial tone phases are measured at the output facet of the MZM to calibrate the lidar. The post-processing algorithm uses the measurement taken at the calibration mirror as the zero point for the lidar system before taking actual measurements of the target. For acquisition, a digital storage oscilloscope is used by setting the time window to 100μs with a 10GS/s sampling rate that yields a time resolution of 0.1nm. Time resolution dictates the range resolution, δL, which is defined by the minimum distinguishable phase of the i^{th} tone, $d\phi_i$, as $\delta L = c \times d\phi_i / \omega_i = c \times dt$. It is possible to formalize the minimum theoretical resolution by considering a noise-free case, where $d\phi_i = \omega_i \times dt$, and hence $\delta L = c \times dt$, where dt is the time resolution. In the case of the experiment, the theoretical minimum resolution is ~3cm without any further post-processing. The target ranges are first computed using the triangulation algorithm after extracting the phase and frequency of the IF tones. Then the extracted tone information is introduced to the ML algorithms to estimate the target range. Subsequently, the PB-MTCW lidar measurements, actual target ranges, and the results of the ML algorithms are compared.

3. MACHINE LEARNING ALGORITHM

After extracting the phase and frequency of the IF tones, we formulate the distance estimation problem based on a basic regression model, mapping a time-series input to a value, to emphasize the relationships between the PB-MTCW and distance. For the proposed basic regression model, the input and output pairs of the ML model are defined as follows. During training, each sample is labeled with the true distance values obtained using the triangulation algorithm. The input of the model is the phase and frequency of IF tones which are extracted as mentioned above.

We denote the extracted phase and frequency values at a point as (ϕ, ω) where ϕ represents the vector formed by the phase values and ω is the number of used tones. The true distance value is denoted as L and obtained by the triangulation algorithm. The designed ML model is parametrized by Φ and the overall regression is given in Eq.(4) where the $\hat{L}$ is the estimated distance value of the target using the input and model parameters. While training the model, we used the L1 loss, which is also known as Mean Absolute Error, and try to minimize the error between model output, $\hat{L}$, and the true distance of the target, L. During the test, the task is to estimate the true distance L given the extracted phase and tone pairs (ϕ, ω) of a sample using the trained model f with parameters Φ, which is shown in Eq.(4). For differentiating the number of targets, the input pair is changed to the magnitude with frequency tones instead of phase. And, the cross-entropy loss is used instead of L1.

The designed regression model takes as input only the phase and frequency tone pairs, and no other raw signal- or system-related features such as the magnitude, or reflection coefficient information are not used in the model to estimate the distance of the target.

$$L = f\left(\phi, \omega, \Phi\right) \tag{4}$$

The regression model has composed of three main layers; the first layer is the input layer and has the twice number of units with the extracted phase values (the phase values and the frequency tones are concentrated horizontally before feeding to the ML model). The second layer is consisted of two hidden layers, which have 256 and 128 units, respectively, and are utilized for extracting features from the input pair. The last layer of the model is the output layer and gives the estimated distance. The network was trained with Glorot initialization of the weights[34]. L2-regularization with 0.001 is applied for each dense layer to prevent overfitting. We used the Adam optimizer[35] with the default parameters $ß_1 = 0.9$ and $ß_2 = 0.999$, and a mini-batch size of 120. The learning rate is initialized to 0.002 and reduced by a factor of 10 when the validation mean squared error stopped decreasing for 75 consecutive epochs. The training continues until 100 successive epochs without validation performance improvements with a maximum of 900 epochs. The best model is chosen as the lowest loss on the validation data. In general, the hyperparameters of the network architecture and optimization algorithm were chosen by manual tuning. We searched essentially over the number of hidden layers and units to find the best model for the estimation.

The evaluation of the ML model is performed on all recorded data without modifying or changing the hyperparameters of the model. The only modification is made for input when the model is try to differentiate whether there are 2 targets or a single target as mentioned before. To evaluate the generalization capability of the trained model, we used the leave distance-out cross-validation, similar to leave-one-out-cross-validation (LOOCV[36]). The used validation method ensures that the trained ML model is capable of generalizing the target distance values which have not been seen by the model during the training. For example, during the training, the model only observes the phase values corresponding to the distances 10-11cm. And, for the inference (test), the phase values at the distance of 10.5cm are fed to the model. In this way, we have followed a principled approach to evaluate the performance of the proposed method.

In the next section, we report our scores of single, non-repeated experiments where the training and validation splitting are performed randomly. 10% of training records were used for validation to implement early stopping based on the validation loss to prevent overfitting. Different percentages are also used while partitioning the validation and training data. However, the best performance has been observed for the 10% of the data for validation and 90% for the training.

4. RESULTS

We performed an extensive set of experiments to test if the proposed method performs well in estimating the target distance values. These tests aimed to evaluate the performance measures and the model's capabilities, in terms of noise level and target distances. The Mean Absolute Error (MAE) and Root Mean Squared Error (RMSD) are used as metrics to evaluate the target distance estimation performance. The metrics are calculated using the estimation values, $\hat{L}$, and the true distance of the target, L, which is obtained by triangulation. The calculation of MAE is shown in Eq.(5) .

$$MAE = \frac{\sum_{i=1}^{n} \left| L_i - L_l \right|}{n} \tag{5}$$

To evaluate the model's performance comprehensively, we changed the distance range of the target, the number of tones with different tone values, and the noise factor. Overall, we performed 3 main experiments which are as follows. 1) Noisy single target distance estimation, 2) Noisy double target differentiation with distance estimation and 3) single target lab environment distance estimation.

For the tone frequency variations, we chose 3 pairs which are $Tones_1$ = [20MHz, 500MHz, 700MHz, 850MHz, 950MHz], $Tones_2$ = [500 MHz, 700 MHz, 850 MHz, 950 MHz], $Tones_3$ = [700MHz, 850 MHz, 950 MHz, 1050 MHz]. By choosing the different number of tones with values, we rigorously evaluated the performance of the machine learning model on the task. Moreover, we have changed the L_1 and L_2, which are the target distance values, with the reflection coefficients of targets. The following three tables summarize the results of our experiments.

Table 1. The estimation errors of the trained ML model for a single target, the first case of the evaluation scheme, evaluated at three different tones with three separate distances.

Tones / L_1 (m)	**0.1-3**	**0.1-5**	**0.1-10**
Tones$_1$	0.0027 ± 0.003 dm	0.0041 ± 0.004 dm	0.0085 ± 0.005 dm
Tones$_2$	0.0029 ± 0.0002 dm	0.0030 ± 0.001 dm	0.0035 ± 0.002 dm
Tones$_3$	0.0013 ± 0.0001 dm	0.0002 ± 0.001 dm	0.0002 ± 0.001 dm

Table 1 shows the average estimation error with standard deviations of the ML regression model that is trained with three different tones which are mentioned before. It can be seen from the data in Table 1 that the proposed ML model with feature extraction can estimate the target distance with high performance. The best performance, which is the average mean error of 0.002 cm, is obtained when the model is trained and evaluated with *Tones*$_3$. Whereas the model's performance decreases by ~10x when it is trained with first tone combinations, which shows the importance of tone selection.

Table 2. The estimation errors of the trained ML model for the first target of the double target, the second case of the evaluation scheme, evaluated at three different tones with three separated distances.

Tones / L_1 (m)	**0.1-1**	**0.1-2**	**0.1-3**
Tones$_1$	0.016 ± 0.05 dm	0.023 ± 0.03 dm	0.031 ± 0.03 dm
Tones$_2$	0.012 ± 0.04 dm	0.014 ± 0.04 dm	0.030 ± 0.04 dm
Tones$_3$	0.006 ± 0.05 dm	0.009 ± 0.001 dm	0.0015 ± 0.001 dm

Table 3. The estimation errors of the trained ML model for the second target of the double target, the second case of the evaluation scheme, evaluated at three different tones with three separated distances.

Tones / L_2 (m)	**3.1-5**	**3.1-7**	**3.1-10**
Tones$_1$	0.025 ± 0.003 dm	0.029 ± 0.005 dm	0.045 ± 0.004 dm
Tones$_2$	0.0053 ± 0.002 dm	0.0067 ± 0.002 dm	0.0071 ± 0.002 dm
Tones$_3$	0.0041 ± 0.001 dm	0.0047 ± 0.001 dm	0.0055 ± 0.003 dm

Tables 2 and 3 show the performance of the model for the case when there are two targets. Therefore, we first evaluated the model's performance for differentiating the number of targets. If the model outputs a single target prediction and there are two targets, we predicted the distance of the first target, and the second target error is reported. In other words, the prediction distance for the second target, $\hat{L}_2$, is set to zero while no modifications have been applied to true distance values. Therefore, the estimation performance of the trained ML models for the double target decreases compared to the single case as can be seen in Tables 1,2, and 3.

When we evaluated the trained model in the classification performance of the number of targets, the accuracy of the classifier is %94±0.7. While evaluating the model, we changed the first and second target distances from 0.1-3 m to 3.1-10 m, respectively. The performance comparison between the Tones, however, has not changed. In other words, when we investigated the performance of the different *Tones*, we can see that *Tones*$_1$ gives the worst result in target distance estimation. This consistency between different experimental setups shows that the ML model's performance is significantly affected by the extracted phase and magnitude values from the pre-processing.

Additional to the overall results (shown in the above tables), we plotted the estimation performance of the ML models against expected distances with two different tones as shown in Figure 3.

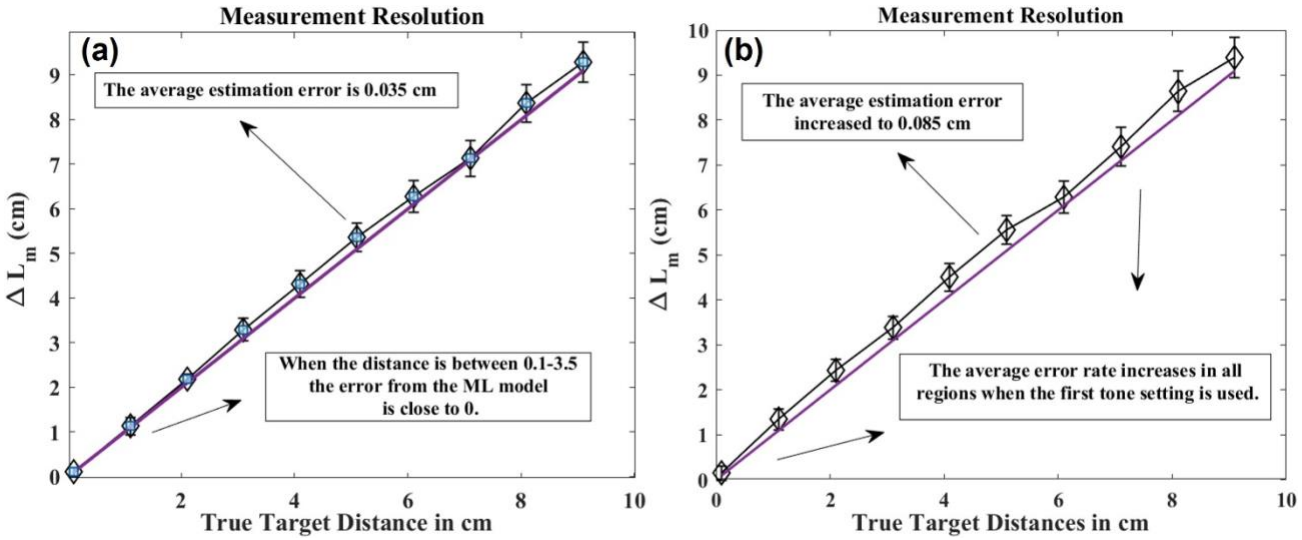

Figure 3. The estimation errors of the trained ML model for different points. A) The case where *Tones*$_2$ is used for both training and testing. B) The case where *Tones*$_1$ is used for training and testing the ML model.

Figure 3 shows the error rate of the ML model for the target distance estimation. The purple line in both graphs represents the perfect estimation case where the error is equal to 0, $\hat{L}$ = L. The black line is drawn with the true target distances against the estimation of the trained ML model. The (a) and (b) plots in Figure 3 show the effect of tone selection on the estimation performance. As shown in this Figure, when *Tones*$_1$ is used for training and testing the ML model, the overall estimation performance decreases by ~ 3x, where this value is higher in long distances. Although this slight degradation in the *Tones*$_1$ is an expected outcome, it can be explained if the frequencies are investigated. In *Tones*$_1$, the first frequency is 20 MHz which is quite low compared to the frequency contents in other tone vectors. Therefore, a performance decrease is observed for this specific tone content.

Lastly, the trained model is evaluated according to scheme three, which is the single target lab environment distance estimation. A small difference between the last experiment and the other two simulations, we had to use a single *Tone vector*, which has 3 frequencies, 500 MHz, 700 MHz, and 950 MHz, during training and testing. The overall estimation error for the last scheme is 0.013 ± 0.01 dm. The major drawback of the third experimental setup is that it requires extensive data collection for training the ML model as the modeling system with machine learning is data-hungry. This drawback limits the extensive experimentation of the model's performance. Therefore, we believe that new solutions should be proposed to train ML models for similar experimental setups.

5. CONCLUSION

This paper introduces the enhancement of the PB-MTCW lidar technique using extracted phase information from different tones. To evaluate our proposed method, we have collected real data with simulations and utilized principled cross-validation for evaluating the Machine Learning model. Our results show that the proposed method predicts the distance in three training schemes with an overall 1.1 mm MSE error.

6. ACKNOWLEDGEMENTS

This work was supported by the Office of Naval Research under grant number # N00014-18-1-2845.

7. REFERENCES

[1] Du, P., Bai, X., Tan, K., Xue, Z., Samat, A., Xia, J., Li, E., Su, H. and Liu, W., "Advances of four machine learning methods for spatial data handling: A review," Journal of Geovisualization and Spatial Analysis **4**(1), 1–25 (2020).

[2] Kotsiantis, S. B., Zaharakis, I. and Pintelas, P., "Supervised machine learning: A review of classification techniques," Emerging artificial intelligence applications in computer engineering **160**(1), 3–24 (2007).

[3] Teri, S. S. and Musliman, I. A., "Machine learning in big lidar data: a review," The International Archives of Photogrammetry, Remote Sensing and Spatial Information Sciences **42**, 641–644 (2019).

[4] Mahesh, B., "Machine learning algorithms-a review," International Journal of Science and Research (IJSR).[Internet] **9**, 381–386 (2020).

[5] Castaño, F., Beruvides, G., Haber, R. E. and Artuñedo, A., "Obstacle recognition based on machine learning for on-chip LiDAR sensors in a cyber-physical system," Sensors **17**(9), 2109 (2017).

[6] Gleason, C. J. and Im, J., "Forest biomass estimation from airborne LiDAR data using machine learning approaches," Remote Sensing of Environment **125**, 80–91 (2012).

[7] Weiss, U., Biber, P., Laible, S., Bohlmann, K. and Zell, A., "Plant species classification using a 3D LIDAR sensor and machine learning," presented at 2010 Ninth International Conference on Machine Learning and Applications, 2010, 339–345, IEEE.

[8] You, C., Lu, J., Filev, D. and Tsiotras, P., "Autonomous planning and control for intelligent vehicles in traffic," IEEE Transactions on Intelligent Transportation Systems **21**(6), 2339–2349 (2019).

[9] Dominguez, R., Onieva, E., Alonso, J., Villagra, J. and Gonzalez, C., "LIDAR based perception solution for autonomous vehicles," presented at 2011 11th International Conference on Intelligent Systems Design and Applications, 2011, 790–795, IEEE.

[10] Yoshioka, M., Suganuma, N., Yoneda, K. and Aldibaja, M., "Real-time object classification for autonomous vehicle using LIDAR," presented at 2017 International Conference on Intelligent Informatics and Biomedical Sciences (ICIIBMS), 2017, 210–211, IEEE.

[11] Urmson, C., Anhalt, J., Bagnell, D., Baker, C., Bittner, R., Clark, M., Dolan, J., Duggins, D., Galatali, T. and Geyer, C., "Autonomous driving in urban environments: Boss and the urban challenge," Journal of Field Robotics **25**(8), 425–466 (2008).

[12] Wallace, L., Lucieer, A., Watson, C. and Turner, D., "Development of a UAV-LiDAR system with application to forest inventory," Remote Sensing **4**(6), 1519–1543 (2012).

[13] Hecht, J., "Lidar for self-driving cars," Optics and Photonics News **29**(1), 26–33 (2018).

[14] Ramasamy, S., Sabatini, R., Gardi, A. and Liu, J., "LIDAR obstacle warning and avoidance system for unmanned aerial vehicle sense-and-avoid," Aerospace Science and Technology **55**, 344–358 (2016).

[15] McManamon, P. F., [LiDAR Technologies and Systems], SPIE Press, Bellingham, WA (2019).

[16] Braun, A., Chien, C., Coe, S. and Mourou, G., "Long range, high resolution laser radar," Optics communications **105**(1–2), 63–66 (1994).

[17] Mourou, G., "The ultrahigh-peak-power laser: present and future," applied Physics B **65**(2), 205–211 (1997).

[18] Rairoux, P., Schillinger, H., Niedermeier, S., Rodriguez, M., Ronneberger, F., Sauerbrey, R., Stein, B., Waite, D., Wedekind, C. and Wille, H., "Remote sensing of the atmosphere using ultrashort laser pulses," Applied Physics B **71**(4), 573–580 (2000).

[19] Behroozpour, B., Sandborn, P. A., Wu, M. C. and Boser, B. E., "Lidar system architectures and circuits," IEEE Communications Magazine **55**(10), 135–142 (2017).

[20] Sandborn, P. A. M., [FMCW Lidar: Scaling to the Chip-Level and Improving Phase-Noise-Limited Performance], University of California, Berkeley (2017).

[21] Lum, D. J., Knarr, S. H. and Howell, J. C., "Frequency-modulated continuous-wave LiDAR compressive depth-mapping," Optics express **26**(12), 15420–15435 (2018).

[22] Godbaz, J. P., Cree, M. J. and Dorrington, A. A., "Understanding and ameliorating non-linear phase and amplitude responses in amcw lidar," Remote Sensing **4**(1), 21–42 (2012).

[23] McManamon, P. F., [Field Guide to Lidar], SPIE Press (2015).

[24] R. Torun, M. M. Bayer, I. U. Zaman, J. E. Velazco, and O. Boyraz., "Realization of Multi-Tone Continuous Wave Lidar," IEEE Photonics Journal, 1–1 (2019).

[25] Dolan, D. H., "Accuracy and precision in photonic Doppler velocimetry," Review of Scientific Instruments **81**(5), 053905 (2010).

[26] Riemensberger, J., Lukashchuk, A., Karpov, M., Weng, W., Lucas, E., Liu, J. and Kippenberg, T. J., "Massively parallel coherent laser ranging using a soliton microcomb," Nature **581**(7807), 164–170 (2020).

[27] Bayer, M. M., Li, X., Guentchev, G. N., Torun, R., Velazco, J. E. and Boyraz, O., "Single-shot ranging and velocimetry with a CW lidar far beyond the coherence length of the CW laser," 26, Opt. Express **29**(26), 42343–42354 (2021).

[28] Bayer, M. M. and Boyraz, O., "Ranging and velocimetry measurements by phase-based MTCW lidar," Opt. Express **29**(9), 13552–13562 (2021).

[29] Bayer, M. M., Guentchev, G. N., Li, X., Velazco, J. E. and Boyraz, O., "Enhancing the multi-tone continuous-wave lidar with phase detection," presented at ODS 2021: Industrial Optical Devices and Systems, 2021, 1182807, International Society for Optics and Photonics.

[30] Peters, R. D., Lay, O. P., Dubovitsky, S., Burger, J. P. and Jeganathan, M., "MSTAR: an absolute metrology sensor with sub-micron accuracy for space-based applications," Proc. of SPIE Vol. 10568, 105682O (2004).

[31] Bhandari, A., Feigin, M., Izadi, S., Rhemann, C., Schmidt, M. and Raskar, R., "Resolving multipath interference in kinect: An inverse problem approach," presented at SENSORS, 2014 IEEE, 2014, 614–617, IEEE.

[32] Bayer, M. M., Atalar, A., Li, X. and Boyraz, O., "Photonics PNT Based on Multi-Tone Continuous Wave Ranging," Conference on Lasers and Electro-Optics, JTh3A.57, Optica Publishing Group, San Jose, California (2022).

[33] Dieckmann, A., "FMCW-LIDAR with tunable twin-guide laser diode," Electronics Letters **30**(4), 308–309 (1994).

[34] Xavier Glorot and Yoshua Bengio. Understanding the difficulty of training deep feed-forward neural networks. In Yee Whye Teh and Mike Titterington, editors, Proceedings of the Thirteenth International Conference on Artificial Intelligence and Statistics, volume 9 of Proceedings of Machine Learning Research, pages 249–256, Chia Laguna Resort, Sardinia, Italy, 13–15 May 2010. PMLR

[35] Diederik P. Kingma and Jimmy Ba, Adam: A method for stochastic optimization. In Yoshua Bengio and Yann LeCun, editors, 3rd International Conference on Learning Representations, ICLR 2015, San Diego, CA, USA, May 7-9, 2015, Conference Track Proceedings, 2015.

[36] Claude Sammut and Geoffrey I. Webb, editors. Leave-One-Out Cross-Validation, pages 600–601. Springer US, Boston, MA, 2010